CEBAF Program Advisory Committee Six (PAC6) Proposal Cover Sheet

This proposal must be received by close of business on April 5, 1993 at:

CEBAF
User Liaison Office
12000 Jefferson Avenue
Newport News, VA 23606

Proposal Title

The 3He(e,e'NN) Reaction

Contact Person

Name: Z. Papandreou
Institution: The George Washington University
Address: 725 21st Street
Address:
City, State ZIP/Country: Washington, DC 20052
Phone: (202) 994 6579 **FAX:** (202) 994 3001
E-Mail → BITnet: zisis@gwuvm **Internet:** zisis@fys.ruu.nl

If this proposal is based on a previously submitted proposal or letter-of-intent, give the number, title and date:

Proposal PR-89-030, "Two-Nucleon Knockout Reactions on 3,4He", 1989

CEBAF Use Only

Receipt Date: 4/5/93 Log Number Assigned: PR 93-011

By: SP

The ^{3}He(e, e'NN) Reaction

The Hall-A and HARP Collaborations

Spokespersons

- *M.B. Epstein, California State University, LA*
- *R.A. Lindgren, University of Virginia*
- *G.J. Lolos, University of Regina*
- *Z.E. Meziani, Stanford University*
- *Z. Papandreou, The George Washington University*

ABSTRACT

We propose to study the two-nucleon knockout reactions ^{3}He(e, e'np) and ^{3}He(e, e'pp) in order to investigate the two- and three-body absorption strength, and short-range correlations in nuclei. The ^{3}He nucleus is selected because it is the lightest non-trivial nuclear system for which realistic wave functions are available, and a triple coincidence renders the experiment kinematically complete. We plan to measure in configurations where the kinematics may permit a simplified interpretation of the data, by selectively emphasizing the various components of the reaction mechanism. An L/T separation is essential in untangling MEC and IC effects, and will be performed as well. We plan to carry out these measurements using the 1-4 GeV CW electron beam at CEBAF and the two high resolution spectrometers in Hall-A for detecting electrons and protons. The third detector arm, which will detect protons and neutrons simultaneously (and thus allow the simultaneous measurement of the above mentioned reactions), will be the High Acceptance Recoil Polarimeter (HARP). HARP, combined with a high power cryogenic ^{3}He target, is capable of operating at luminosities of 10^{38} cm^{-2}s^{-1}, making this experiment feasible.

Participants

G.J. Lolos and G.M. Huber
Department of Physics, University of Regina, Regina SK S4S 0A2 Canada

B.L. Berman, W.J. Briscoe, P. Cole, K.S. Dhuga, W.R. Dodge, Z.Papandreou and S. Rugari
Department of Physics, The George Washington University, Washington DC 20052

H. Baghaei, D. Crabb, D. Day, R.A. Lindgren, R.W. Lourie, J. McCarthy, and O. Rondon-Aramayo
Department of Physics, University of Virginia, Charlottesville VA 22901

K.A. Aniol, M. Epstein and D.J. Margaziotis
Department of Physics, California State University, Los Angeles CA 90032

D. Kawall and Z.-E. Meziani
Department of Physics, Stanford University, Stanford, CA 94305

Th.S. Bauer, H.W. den Bok and H.W. Willering
Department of Subatomic Physics, Utrecht University, 3508 TA Utrecht, The Netherlands

J.A. Tjon
Institute for Theoretical Physics, Utrecht University, 3508 TA Utrecht, The Netherlands

E. Voutier, J.P. Bocquet, C. Furget, J.C. Gondrand, S. Kox, F. Merchez, C. Perrin and D. Rebreyend
Institut des Sciènces Nucléaires de Grenoble, F-38026 Grenoble, France

P.E. Ulmer and J. Mitchell
Physics Division, CEBAF, Newport News VA 23606

J.J. Kelly, H. Breuer, P. Markowitz, T. Payerle
Department of Physics, University of Maryland, College Park, MD, 20472

G. van der Steenhoven, J.L. Visschers, D. Ireland, M.A. van Uden
NIKHEF-K, P.O. 4395, 1009 AJ Amsterdam, The Netherlands

S. Frullani and F. Garibaldi
INFN/Rome, Rome, Italy

R. de Leo, A. Leone and R. Perrino
INFN/Lecce, Lecce, Italy

1 Introduction and Survey of the Field

1.1 Experimental Evidence for Multi-nucleon Correlations in Nuclei

The successes of electro-nuclear scattering, both inclusive and exclusive, are largely based on the simplicity of the underlying mechanism and the exactness of the electron-nucleon coupling mechanism. Such a picture of e-nucleon and e-nucleus interactions is largely based on diagrams as the one shown in Figure 1a. This mechanism is perturbative and allows the separation of the reaction mechanism from that of nuclear structure. Even in the simplest nucleus, however, the need for other diagrams arose in order to account for the experimental data. This is clearly illustrated for the ^{2}H(e, e')pn reaction [1], for example, where it is necessary to include additional mechanisms such as meson exchange currents (MEC) (Figure 1d), $\pi + \rho$ exchange, as well as the Δ resonance (IC).

Even though the e-nucleus reaction can be approximated, to first order, by the incoherent sum of the elementary e-N interactions, in practical terms certain complications arise due to the presence of the other nucleons in the nucleus. The easiest of these complications to understand, although not as easily dealt with, is that of Final State Interactions (FSI) between the struck nucleon and the rest of the nucleus. One such diagram of FSI is shown in Figure 1c. In principle this reaction is uninteresting since it involves secondary rescattering among the struck nucleon and one or more spectator nucleons. In terms of the results, however, these processes modify the four momentum of the struck nucleon, thus altering the flux in any particular kinematical region.

The (e, e'p) reactions have been used extensively in electro-nuclear physics, to extract the single nucleon form factors in the nucleus, but these reactions have shed little light on medium modifications due to FSI. The same (e, e'p) data have also been used extensively in hadron physics to model the momentum distributions of nucleons in nuclei, in order to extract information from Monte Carlo simulations of hadronic nucleon-knockout reactions.

In principle the quasi-elastic region, as shown in Figure 3, is best suited for such studies, as long as FSI are properly accounted. However, there is a growing body of evidence [2, 3] for the existence of two-nucleon effects even in this region. Certainly, the picture of e-nucleus interactions based on the diagrams of Figure 1a, c and d, starts breaking down as the energy transfer, ω, increases past the quasi-elastic region. In the "dip" region (between the Q.E. peak and the single nucleon excitation known as the Δ resonance), the experimental data clearly indicate more strength than the basic e-p interaction can account for as shown in Figure 4.

Further evidence supporting the existence of more complex mechanisms has been gathered in both inclusive (e, e') and semi-inclusive (e, e'p) experiments. In the case of the ^{40}Ca(e, e') reaction [4] the separated longitudinal response function, shown in Figure 5, exhibits a lower strength than predicted by the independent

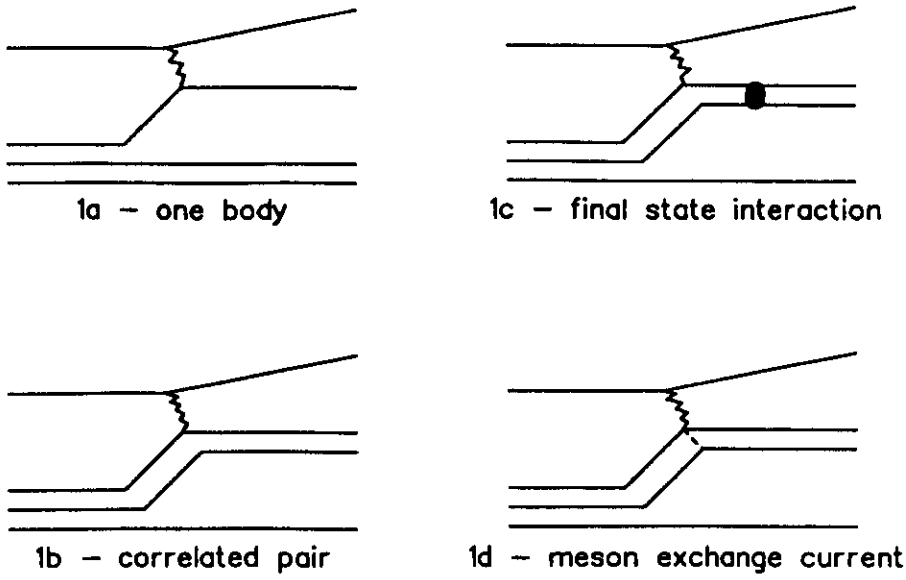

Figure 1: Diagrams contributing to electron-nucleus interactions.

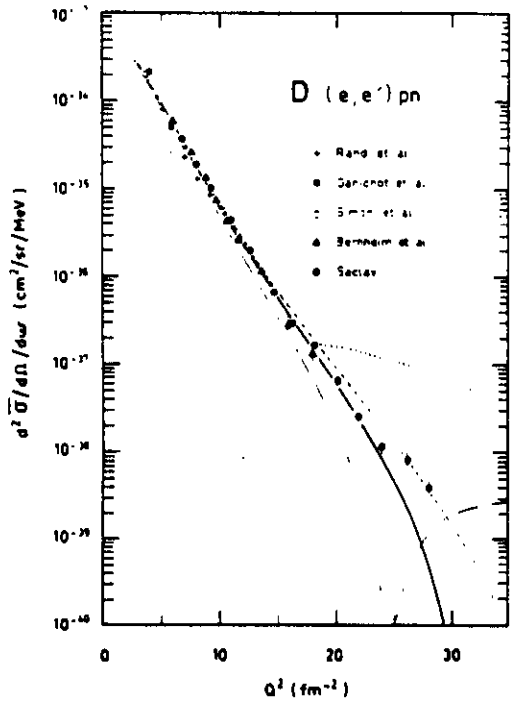

Figure 2: ^{2}H(e,e')pn data and the contributions of the various diagrams from Figure 1 [1]. The dotted curve represents the impulse approximation, the dash-dotted curve includes the pion exchange contribution, and the dashed curve includes in addition the ρ-exchange diagram. The solid curve is the total result, in which the Δ-isobar current is included as well.

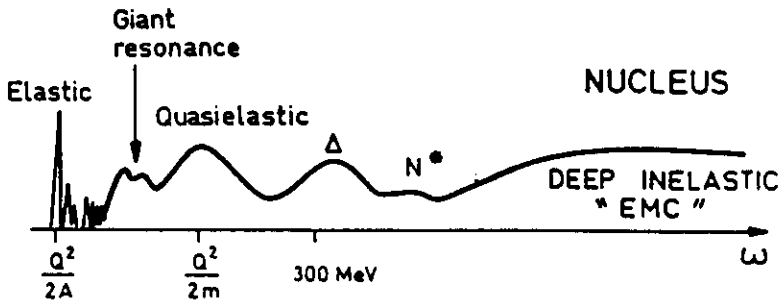

Figure 3: Schematic drawing of an inclusive electron-nucleus energy loss spectrum.

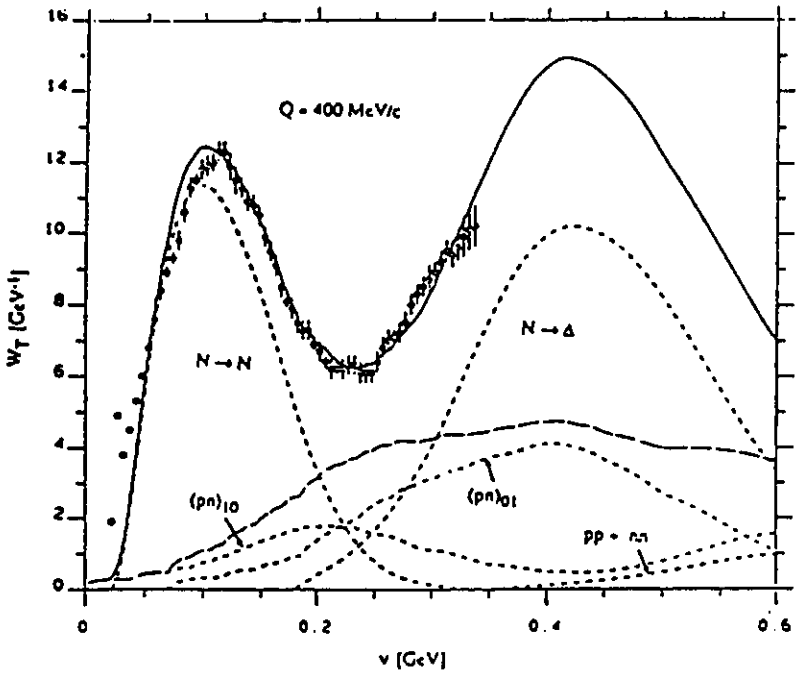

Figure 4: Experimental data and the result of different amplitudes included in the calculation.

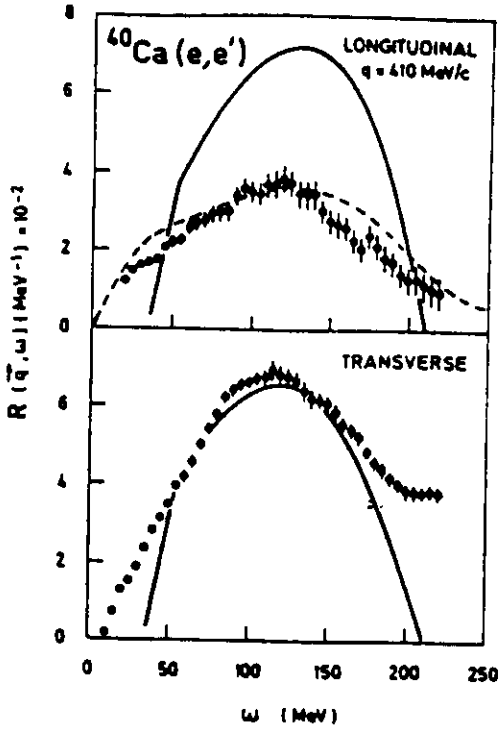

Figure 5: Longitudinal and transverse response functions on ^{40}Ca at q=410 MeV/c. Solid curve: Fermi gas prediction; dashed: result of a calculation for nuclear matter which includes correlations.

particle models of Figure 1a. Also, evidence for multi-nucleon processes has been documented in the ^{3}He(e, e'p) reaction [5] resulting in broad peaks in the missing energy spectra as shown in Figure 6. Based on the kinematical and dynamical behaviour of the data, these authors conclude that the broad peak is a signature of the interaction of the incoming virtual photon with a correlated nucleon pair in ^{3}He, as shown schematically in Figure 1b.

In the case of absorption experiments with real photons, the evidence of real photons being absorbed on correlated pairs of nucleons is overwhelming. The absorption of the photon by a T=0 pair of nucleons, commonly referred to as quasi-deuteron absorption, has been clearly seen experimentally [6, 7]. More recently, results by the TAGX collaboration for the ^{3}He(γ, pn)p reaction [8], using tagged photons, are consistent with the quasi-deuteron absorption model as shown in Figure 7. As can be seen in this figure, the emitted neutron and proton are strongly correlated in momentum space while the missing momentum (the momentum of the unobserved proton) is consistent with that of a spectator nucleon. One should note that the absense of such a low energy peak in the neutron momentum distribution indicates a much smaller cross section for the ppn final state, in which the neutron acts as a spectator. In addition, the neutron and the proton exhibit a different angular distribution depending on whether one of the protons is a spectator or a participant, consistent with multinucleon absorption. These data have produced unambiguous evidence for photo-absorption by three nucleons (3NA) with a constant matrix element, as defined by a three-body phase space di ribution. A similar picture was observed for the more inclusive data measured re ıtly at Brookhaven [9], as shown in Figure 8, where 2N+3N fit the data better ıan 2N alone. It is, of

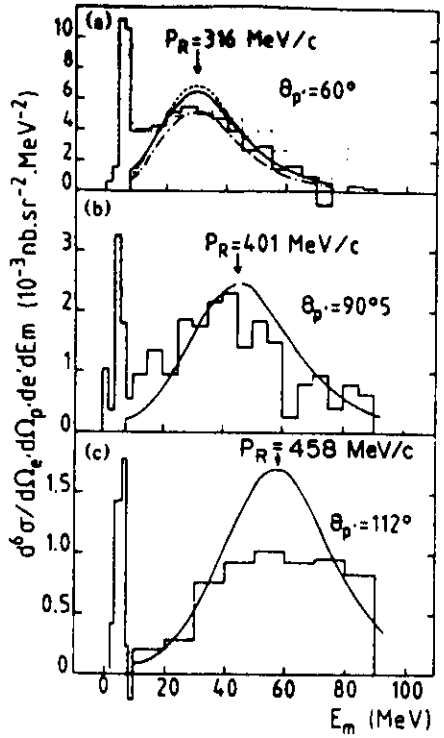

Figure 6: Missing energy spectra in the ^{3}He(e, e'p) reaction. The solid line indicates the result of a DWIA calculation with the inclusion of MEC.

course, not surprising that a real photon needs at least two nucleons to absorb its four momentum due to the large momentum mismatch between the photon and the bound nucleon.

The absorption of real photons by nuclei is very similar in nature to pion absorption on nuclei, where absorption on the T=0 (pn) pair dominates the absorption channel. The main difference is that photo-absorption is a volume phenomenon while pion absorption in the resonance region is understood as a surface effect. This holds particularly true for medium to heavy nuclei. In the reactions of the type A(π, NN)X, the investigations have been centered on the contribution to the total absorption cross section by 2NA, 3NA and even 4NA. The issue of multi-nucleon absorption has been reduced to, not if, but how much, and the relevant publications are too numerous to mention here. As an example, the ^{4}He(π^+, ppp)n [10] and ^{3}He($\pi^\pm$, NNN) [11] results in Figure 9a, b, respectively and the references therein present a clear picture of this issue. They also point to a large (30 %) contribution by 3NA to the total absorption cross section at resonant energies! One element of note in the pion absorption field is the sophistication of the detector and analysis techniques, such as the use of Dalitz plot analysis, to compare the Monte Carlo simulations to the data (see Figure 9).

Even though the CW beams of the meson factories allowed a wealth of pion scattering and pion absorption data, the strong interaction of the pion with the mean field of the nucleus, before absorption proper takes place, complicates the interpretation of the data. Off-shell effects for the pion are more serious than those for the nucleon due to its smaller mass [12] and, as such, initial state interactions (ISI) cannot effectively be modeled, unlike FSI [10, 11]. This fact alone emphasizes the importance of (γ, NN) and (e, e'NN) reactions that do not suffer from ISI and

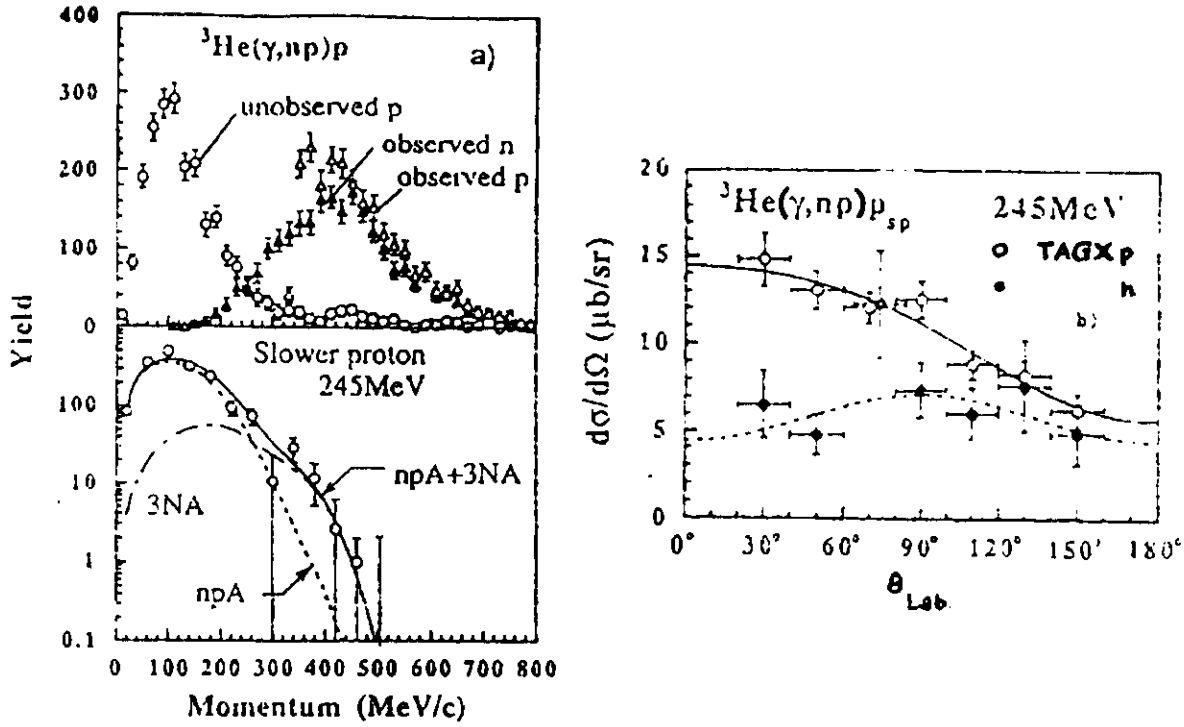

Figure 7: (a) Momentum distributions for the observed proton (open triangles), the observed neutron (solid triangles) in the TAGX trigger and that for the unobserved (missing momentum) proton (open circles) in the ^{3}He(γ, pn)p reaction and (b) dσ/dΩ angular dependence for the neutron (solid circles) when the proton acts as a spectator and the proton (open circles) which can be either a spectator or a participant [8].

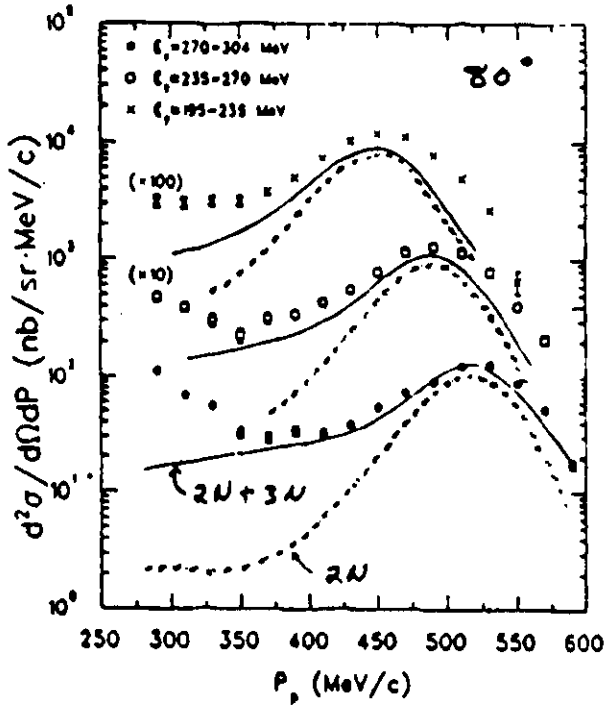

Figure 8: Momentum distribution of the proton in the ^{3}He(γ, p)p reaction. The curves are by Laget and include FSI but not π-production [9].

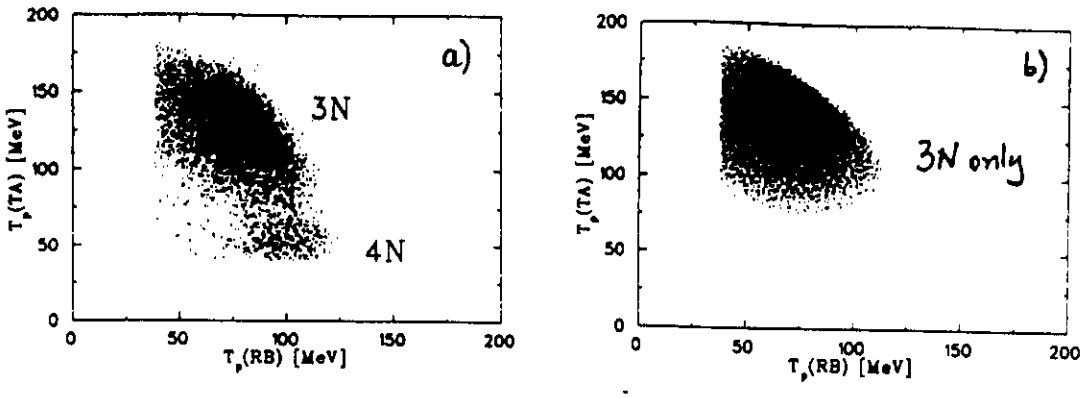

Figure 9: Energy plot for a) data and b) Monte Carlo simulation, for the ^{4}He(π, ppp)n reaction [10]. 3NA and 4NA contributions are shown.

thus can probe short range correlations in the nucleus more effectively.

The complexity of the above mentioned interactions dictates the need to combine the information from pions and photons (real and virtual). The common underlying physics between pion and photon (on- or off-shell) absorption is clearly demonstrated by the same shape of the distributions, for very similar energy and momentum transfers, in the (e, e'p) [13] and (π^+, p) [14] reactions as shown in Figure 10. The characteristics of each probe establish them as complimentary tools in the investigation of nuclear interactions. The pions are associated with substantial cross sections, surface effect sensitivity, a fixed relationship between ω and q, clean experimental environment, but complicated and non-perturbative interactions with nucleons with the addition of ISI complications. The real photons are characterized as a volume probe with understood γ – N coupling, no ISI and fixed ω-q. Virtual photons are similar to real photons but ω and q can be varied independently and allow for the separation of the longitudinal and transverse response functions which is not possible with real photons and pions. For a more detailed comparison of these probes, the reader is directed to reference [15].

1.2 The Theoretical Evidence for Multi-nucleon Correlations

Calculations employing only a one-photon exchange mechanism (Figure 1) fail to describe the quenching of the separated longitudinal response function in (e, e') experiments on ^{40}Ca, ^{48}Ca and ^{56}Fe [4]. Of the several mechanisms proposed to explain this phenomenon (e.g. relativistic effects, MECs, correlations among nucleons, "swollen" nucleons in nuclear matter, etc.), no single one can describe the observed discrepancy; rather a combination of several mechanisms appears to be required.

The various theoretical calculations seem to emphasize different aspects of the reaction mechanism. In Figure 5, the inclusion of nucleon-nucleon correlations have proven more successful as shown by the dashed curve. In Figure 11, relativistic

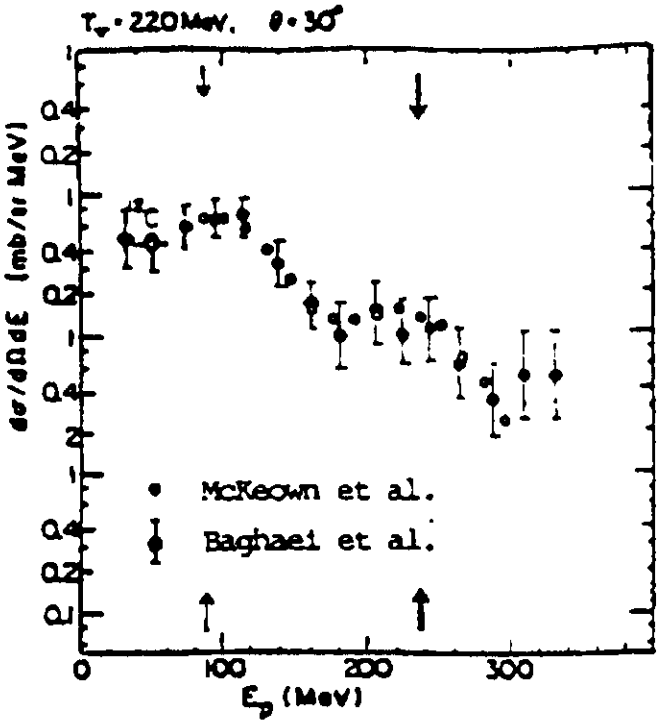

Figure 10: Yields as a function of the energy of the emitted proton in the $^{12}C(e,e'p)$ reaction [13] and the $^{12}C(\pi^+,p)$ reaction [14] (see reference [15]).

MECs coupled to medium modified masses for the nucleon and the Δ seem to describe the data well, even in the dip region. The enhancement of the cross section at large missing energies observed in the $^{12}C(e,e'p)$ reaction [17] has been addressed by theory but the conclusions were that diagrams (a) and (c) of Figure 1 cannot account for the missing energy in the data [18]. Inclusion of 2NA, however, also failed to adequately explain the experimental features thus suggesting 3NA or even more complicated processes [18], although these last calculations were performed in the static limit assuming a constant matrix element for the photon coupling and should be taken cautiously. To illustrate this point, both the static and non-static limit curves are shown in Figure 11.

The theoretical situation is very similar for (γ,NN) reactions as well. Of particular - but not exclusive - interest to real photon absorption, is the issue of existence of three body forces (3BF). Such forces can manifest themselves in atomic systems (Holstein- Primakoff mechanisms) [19] as well as nuclear systems [20, 21]. Such 3BF involve two non-sequential meson exchanges and cannot be constructed by any summation of pair-wise potentials. So far no conclusive evidence of 3BF effects has been observed in $^3He(\gamma,pp)n$ reactions at SAL [22], Saclay [23] and TAGX [8]. However, the results from [8] seem to confirm the theoretical prediction [24] that the 2NA (pp) takes place through the E2 transition, and that the radial wave function of the (pp)-pair in ^3He is similar to that of the (pn)-pair in the deuteron, and thus it is known.

Although the quantity and the quality of pion absorption data far exceeds those available in photo-absorption, the theoretical models dealing with multi-nucleon correlations are not all that impressive. This reflects the ISI issues raised earlier on

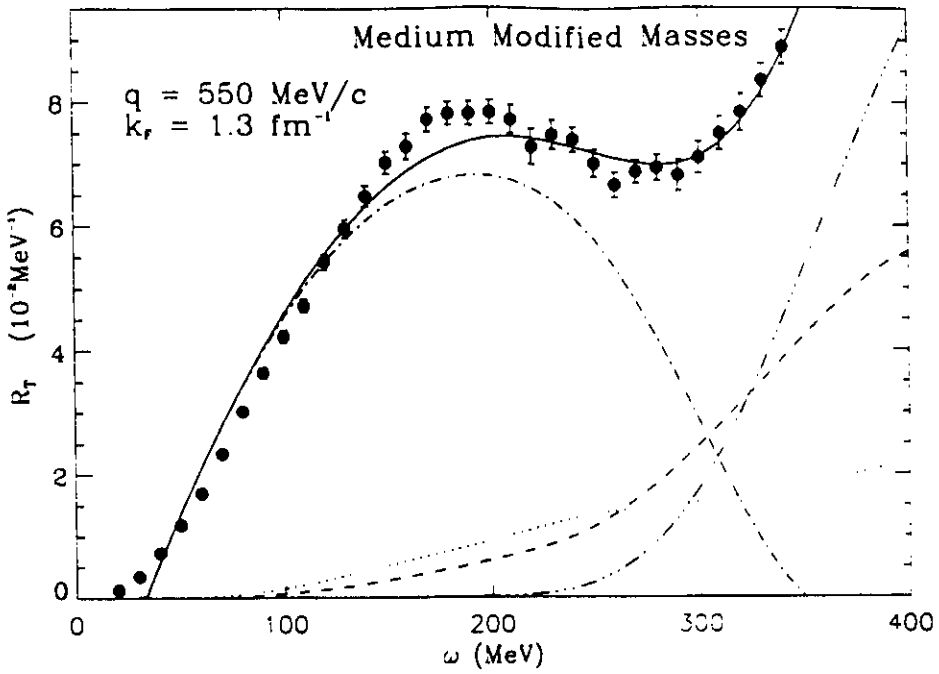

Figure 11: Calculations from reference [16]. Dash-dotted curve: one-body nucleon response including interference with two-body currents, dash-triple-dotted: one-body Δ response, dashed: non-static total two-body (including Pauli exchange) contribution, dotted: static limit (non-relativistic) two-body for purposes of comparison. The solid curve is the full result.

and the complictaed nature of the pion-nucleon coupling in the nuclear medium. In addition, the early experimental indications from pion absorption on light nuclei were that the T=0 channel accounts for the angular distributions and magnitudes of the differential cross sections. DWIA calculations were deemed sufficient to account for the observed reaction mechanism. Some additional mechanisms of pion absorption involving the double-Δ [25] and 3NA [26] have been proposed as alternatives in order to account for the mounting experimental evidence of multi-nucleon role. The double-Δ, which can decay into four nucleons, has not been experimentally identified yet. Perhaps the most comprehensive microscopic calculations are those of [26] where 2NA and 3NA diagrams were included as part of the reaction mechanism. The contribution by 4NA was judged to be too small, by phase space considerations when Pauli blocking is taken into account, and was ignored. The results are generally in good agreement with the data for two nucleons in the final state but the 3NA contribution is overestimated compared to the available data. The inclusion of quark-gluon degrees of freedom in a one step 3NA [27] is claimed to account for the 30 % effect due to 3NA observed in references [10, 11].

2 The (e, e'NN) Reaction

2.1 Scientific Motivation

In nuclear reactions where two nucleons are emitted, information on the two-hole spectral density function and the two-body density matrix [28, 29, 30, 31] can be obtained. From such investigations one hopes to extract the two-body density in the ground state of the target nucleus and thus obtain an understanding of dynamical short-range correlations which are essential for a proper description of nuclear structure.

In the case where two nucleons are emitted in a (e, e'NN) or (γ, NN) reactions, one can describe the measured differential cross section in terms of structure functions, which represent the response of the nucleus to the longitudinal and transverse components of the photon in the interaction. These structure functions depend only on the kinematical quantities ω, q and the angles between the momentum transfer q and the individual particle momenta p' of the two emitted nucleons, and are linear combinations of the hadronic tensors $W^{\mu\nu}$ [31]:

$$W^{\mu\nu} = \sum_{if} \int (J^{\mu}(\vec{q}) J^{\nu *}(\vec{q}) \delta(E_i - E_f) \tag{1}$$

$$J^{\mu}(\vec{q}) = \int < \Psi_f | \hat{J}^{\mu}(\vec{r}) | \Psi_i > e^{i\vec{q}\cdot\vec{r}} d\vec{r} \tag{2}$$

The transition matrix element in equation (2) consists of the one- and two-body parts of the current operator, $J^{(1)}$ and $J^{(2)}$, respectively:

$$J^{\mu}(\vec{r}, \vec{r}_1, \vec{r}_2) = J^{(1)\mu}(\vec{r}, \vec{r}_1) + J^{(1)\mu}(\vec{r}, \vec{r}_2) + J^{(2)\mu}(\vec{r}, \vec{r}_1, \vec{r}_2) \tag{3}$$

where $\vec{r}$, $\vec{r}_1$, $\vec{r}_2$ are the coordinates of the recoiling nucleus and the two ejected nucleons, respectively.

The one-body operators $J^{(1)}$ can contribute to two-nucleon emission only via short-range correlations. The two-body current operator $J^{(2)}$ can produce two-nucleon emission even if these two nucleons are not correlated. As such, $J^{(2)}$ may or may not include correlations but it is important, nonetheless, because it contributes to the two-body absorption of the γ (real or virtual).

The amplitude $J^{\mu}(\vec{q})$ [32] depends on the Jastrow-type correlation function $g(|\vec{r}_1 - \vec{r}_2|)$, which contains among other terms an isospin independent central term and isospin dependent spin and tensor terms. For the ^{16}O(e, e'pp) reaction, a N-N interaction with a large hard-core value of c=0.6 fm greatly enhances the cross section expected from $J^{(1)}$ while a soft-core N-N interaction with c=0.5 fm produces a smaller cross section, as shown in Figure 12. This is connected to the fact that $J^{(1)}$ can only produce two nucleons through such short-range dynamical correlations.

The $J^{(2)}$ operators include MEC and IC terms and thus can eject two nucleons even if short-range correlations are not included. It has been shown [31] that the

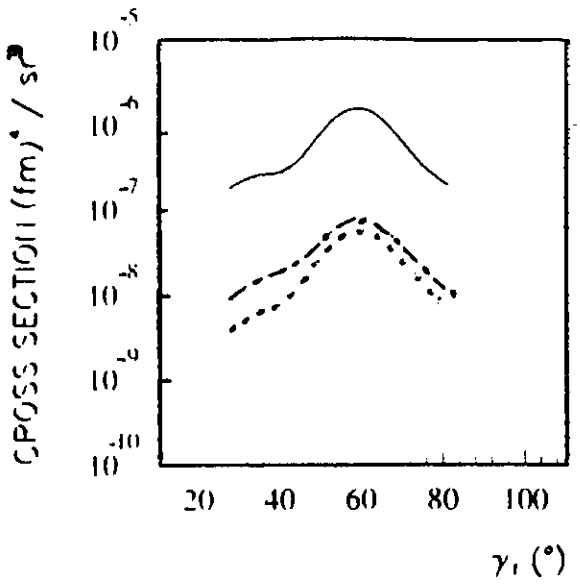

Figure 12: Cross-sections for the ^{16}O(e,e'pp) reaction in coplanar symmetrical kinematics. The parameters are E=700 MeV, ω=150 MeV and q=400 MeV/c. The solid line is the result of the full calculation including $J^{(1)} + J^{(2)}$ terms with hard-core potential. The dot-dashed line is similar calculation with soft-core potential. Dashed and dotted lines represent the results of the calculation based only on the $J^{(1)}$ terms with hard-core and soft-core potentials, respectively, taken from reference [31].

choice of N-N interaction has opposite effects on the $J^{(2)}$ than it has on the $J^{(1)}$ operators. The hard-core interaction decreases the contribution of $J^{(2)}$, unlike for $J^{(1)}$, while the assumption of soft-core N-N interaction has the opposite effect on these terms. As such, the one-body operators are more sensitive to short-range N-N correlations in nuclei than the $J^{(2)}$ two-body terms. As a result, the cross section for the (e,e'pp) reaction depends essentially on correlations, while for the (γ, pp) reactions both effects are important [31] due to the transverse and longitudinal contributions to the IC in this case.

In summary, while (e,e'p) reactions probe the nucleon distributions within the mean field of the nucleus, (e,e'pp) reactions probe short-range correlations in nuclei. Such correlations are important for all aspects of nuclear properties including the one-body operators which define the momentum distribution of the nucleons. A systematic study of (e,e'pp) and (γ, pp) reactions is absolutely vital as only such reactions are constraining enough for the task at hand. Missing energy arguments in (e,e'p) reactions only hint at the problem, as they can not constrain $J^{(1)}$ or $J^{(2)}$ in any nucleus more complex than deuteron. The ^{2}H(e,e'p)n reaction provides some information on $J^{(1)}$ and $J^{(2)}$ but, due to the nature of deuteron, short-range correlations are practically non-existent, with the exception at high recoil momenta where there is an appreciable overlap of the wave functions of the two nucleons.

Although the question of short-range correlations is an important one, the question of the total strength of $J^{(1)} + J^{(2)}$ terms is also important as part of our

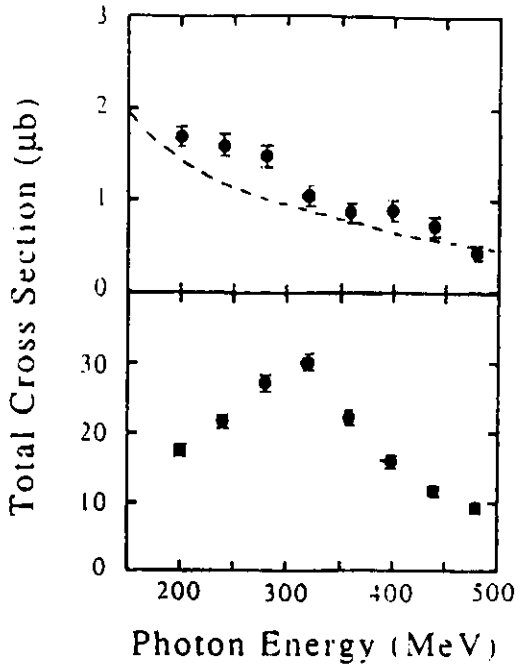

Figure 13: Total cross-sections as a function of incident tagged photon energy for (a) two-body absorption leading to a 2p final state and (b) for the three-body absorption leading to ppn final state in the ^{3}He(γ, pp)n reaction from reference [8]. The dashed line in (a) is from reference [24], for photo-absorption on a pp bound pair assuming E2 transition and pn-like radial wavefunction.

need to understand the (e, e′) reaction in its totality. Knowing that some strength is unaccounted for by the basic (e, e′N) amplitudes is not enough, and a determination of the exact nature and dynamical properties of the A(e, e′) should be explored. An additional issue is that of three-body currents resulting in three-nucleon emission in the reactions (e, e′NNN) and (γ, NNN). In addition to three-body currents $J^{(3)}$, such signatures can be accounted for either by 3BF, as mentioned in section 1, or by a combination of $J^{(2)}$ terms and short-range correlations. Three-nucleon emission following photon absorption, is by no means a small effect as indicated in Figure 13. The data in Figure 13b has been extracted from the ^{3}He(γ, pp)n reaction and satisfy neutron momentum distributions consistent with three-body phase space. The total three-body cross section is clearly more than an order of magnitude larger than the 2p absorption.

2.2 The Choice of Target Nucleus (^{3}He)

The choice of target is most often a compromise among many conflicting requirements. The nature of short-range correlations dictates a target of high nuclear matter density, like ^{4}He and other light nuclei, with a good description of the nuclear wave functions in the initial and final states. As such, ^{4}He is particularly attractive and should be part of such a program. When the requirement extends to the determination of the $J^{(2)}$ terms and three-body currents, as well as investigation of 3BF, the reaction ^{4}He(e, e′NN) is not exclusive enough to constrain the data. One should keep in mind that four-body phase space is similar to three-body phase

space, and therefore the reaction mechanism can not be reliably extracted from missing momentum and energy distributions alone. This has been repeatedly shown in pion absorption investigations, where the detection of three nucleons following pion absorption on ^{4}He [10] was necessary. This task becomes even more complicated for heavier nuclei, which in addition may suffer from increased FSI complications. Some exploratory measurements on the ^{12}C(e,e'pp)n reaction have been made [15], although due to the limited statistical accuracy no conclusions could be drawn.

As such, ^{3}He is a very attractive target: it has well described ground state and continuum wavefunctions, the reaction ^{3}He(e,e'NN)N is kinematically complete and in fact over-constrained, and one can probe effectively one-, two- and three-body currents with reduced and calculable FSI effects. The inter-nucleon distance is not that much smaller than heavier nuclei and thus the short-range correlation signatures are strong enough to manifest themselves if one believes the theoretical assumptions. ^{3}He is in this respect a bench mark test of the new generation of experiments, in the respect that if we hope to ever understand multi-nucleon correlations in nuclei, **we must be able to account** for the ^{3}He case in (e,e'NN) reactions. It is the stepping stone to ^{4}He and ultimately to heavier nuclei.

2.2.1 The ^{3}He(e,e'pn)p Reaction

The absorption of the virtual photon on a pn-pair is dominated by MEC and IC in the $J^{(1)}$ and $J^{(2)}$ terms, which are intertwined with short-range correlations thus making the extraction of $J^{(1)}$ terms more calculation dependent. It is expected that due to its strength compared to (e,e'pp) reaction channel, the pn-channel will dominate the multi-nucleon absorption channels, and hence merits a thorough study. In addition, it should be accurately measured to determine any interference with the pp-channel via FSI. As mentioned above, the TAGX results indicate significantly higher three-nucleon absorption cross section than two-nucleon on pp [8] in ^{3}He, and therefore it is important to measure the ^{3}He(e,e'pn)p channel, as it will determine both the quasi-deuteron and three-body absorption cross sections under the same systematic experimental conditions. This, incidentally, is the situation with pion absorption on ^{3}He, where the T=1 channel has a lower total cross section than absorption on a T=1/2 (NNN) channel. Even though the ^{3}He(e,e'pn)p reaction contains MEC and IC terms, under appropriate kinematical conditions like anti-parallel and coplanar kinematics, it yields the same information on short-range correlations as (e,e'pp) reactions. However, the pn-channel is not as sensitive to correlations because MEC contributions have to be subtracted. On the other hand, at kinematics where the unobserved proton acts as a spectator, and where the cross sections are higher than the pp-channel, one has an excellent opportunity to search for interesting three-nucleon effects such as 3BF.

2.2.2 The ^{3}He(e, e'pp)n Reaction

The (e, e'pp) reaction is, to first order, free of MEC contributions and thus is a better tool for investigating short-range interactions. It contains IC terms but with suitable choice of kinematics these can be enhanced or diminished. Reduction of the IC contributions is critical because their presence greatly affects the choice of N-N interaction assumed, hard-core or soft-core. In the formulation of reference [31], the sensitivity of the selected kinematical region is negligible, assuming a hard-core interaction, while for soft-core a much higher sensitivity is observed. Such selective choice of kinematical regions is coupled to the small cross sections and it is sensitive to two-step competing processes.

In order to minimize IC effects one has to minimize the transverse and interference components of the nuclear response. In general, there are six response functions which contribute to the cross section for this reaction. Confining the ejectiles in-plane reduces these response functions to four. The further requirement of super-parallel kinematics [32], allows only two functions to survive: the longitudinal and the transverse. Therefore, coplanar and anti-parallel kinematics with high polarization, ϵ, values for the virtual photon must be chosen. However, since even at forward angles the transverse component still contributes, a proper L/T separation must be performed to disentangle the various contributing mechanisms. The statistical requirements, due to the low cross sections, demand experiments with high luminosity and the use of three detectors which can all operate in such an environment. For these reasons, Hall-A is the most suitable area at CEBAF to carry out these experiments.

2.3 The Effects of FSI

The question of FSI and the modification of the observables under consideration has been an issue of controversy. The pion absorption data base does not provide accurate numbers on the magnitude of FSI. In reference [11], the total absorption cross section for the ^{3}He($\pi^{\pm}$, NN)N for all combinations of p and n detected, clearly identified FSI contributions. Such FSI are realized as soft final states (low relative angular momentum for the two nucleons) and hard FSI such as rescattering and charge exchange. The contribution of such processes to the total absorption cross section was found to be smaller than the uncertainty on this cross section [11], and decreases with increasing pion energy (i.e increasing nucleon energy as expected from N-N scattering).

The systematic search for ISI and FSI effects in pion absorption at TRIUMF and KEK, concentrated on the (π^-, pp) reaction. Such a reaction cannot proceed through 2NA, and absorption on a T=3/2 (ppp) cluster is suppressed by the Pauli exclusion principle, which does not allow s-states of relative angular momentum. The results by KEK indeed identified peaks in the pp angular distributions, which were attributed to π − N and N-N ISI and FSI respectively [33]. The TRIUMF results, however, with better particle identification and background rejection ob-

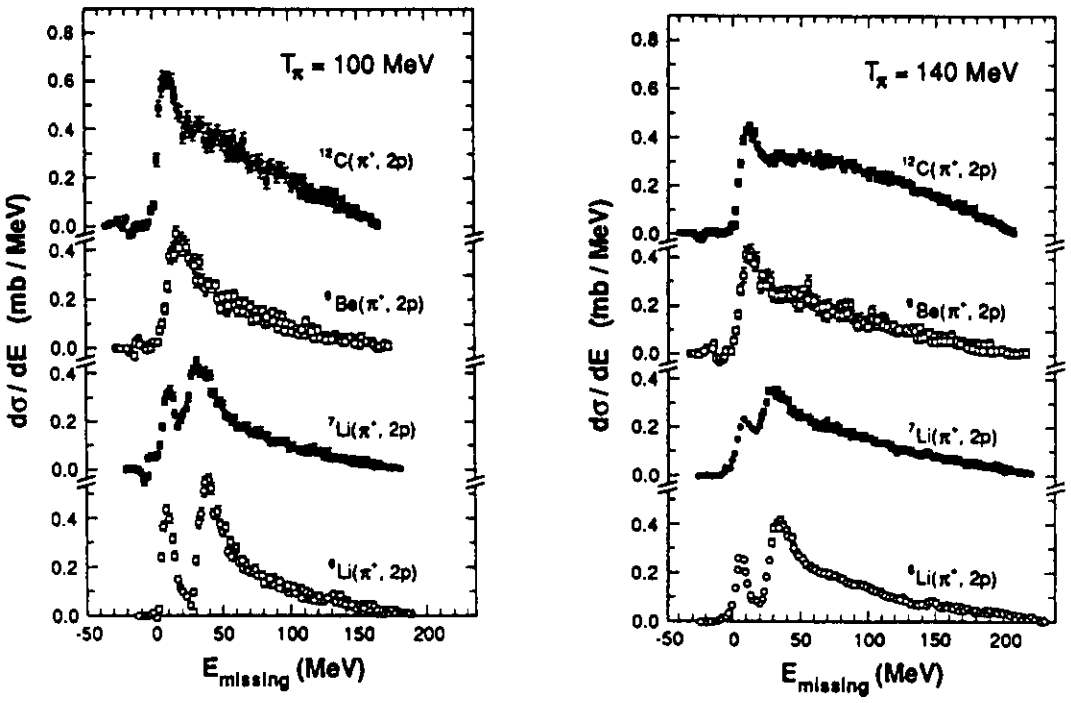

Figure 14: Pion absorption cross sections as a function of missing energy for targets from ^{6}Li to ^{12}C for a) 100 MeV and b) 140 MeV incident pions.

served no such effects, and the pp opening angle distributions were free of such correlations, following instead three-body phase space distributions [34]. A more elaborate experiment [35] based on the same reaction has been completed and is under analysis, employing energy as well momentum distributions, in addition to angular correlations, in order to disentangle this issue.

Pion absorption results from LAMPF [36] seem to indicate that FSI do not play a major role, as displayed in Figure 14. In going from ^{6}Li to ^{9}Be there is a 50 % increase in the number of nucleons (a 75 % increase in residual nucleons following two-body absorption), and one would expect an increase in cross section in the high missing energy region due to FSI. However, only a very small difference is observed between the ^{6}Li and ^{9}Be spectra in this region. Furthermore, there is a large increase in strength between the 100 MeV and 140 MeV ^{12}C high energy tails. This is not consistent with FSI, if the latter follow the free nucleon-nucleon cross sections, nor with ISI, due to the large missing energy and small cross sections. The high missing energy tail is best accounted for by a large three-nucleon absorption constribution.

The data from TAGX on ^{3}He(γ, pn)p in Figure 7, also show very little evidence for FSI modifying the momentum distribution of the unobserved proton. The absence of any significant high momentum components, is interpreted as lack of FSI between the detected p and n as well, as between the detected and the undetected

particles. In conclusion, despite deliberate searches for FSI in pion absorption, and data from electronuclear reactions of the kind pursued in this proposal, we have failed to identify such effects to significantly alter the conclusions about the reaction mechanism.

Finally, on the theoretical front, "exact" calculations on ^{3}He support the argument that the FSI contribution is small. These calculations [37] employ the Faddeev method for calculating the ground state and continuum wave functions of ^{3}He, and apply relativistic kinematics for the outgoing nucleons. In the kinematical domain of this proposal, the FSI contribution for the ^{3}He(e, e'pn)p and ^{3}He(e, e'pp)n reactions is on the level of 10 to 15 %. In reference [38], distortions leave the shape of the cross section unaffected and only produce a change in its magnitude which depends on the particular optical potential chosen for the calculations.

2.4 Summary and Conclusions

2.4.1 Summary

We propose to measure and determine the two- and three-nucleon photo-absorption channels and extract the role of nucleon-nucleon correlations in ^{3}He. The levels of statistical and systematic accuracies aimed at in this proposal, reflect the physics driving the nucleon correlations and their dependence on their kinematic variables. The reasons why we believe we will accomplish these goals are summarized below while addressing, at the same time, the comments by the original PAC that reviewed the version of this proposal submitted in 1989.

- The physics of nucleon correlations in light nuclei does not need any more survey measurements of the (e, e'NN) type, as far as the physics addressed in this proposal is concerned. No one disputes the existence of two-body currents and the role which three-nucleon absorption plays in similar reactions. Pion absorption, during the last 10 years, has provided us with a wealth of both survey and precision results. Real photon absorption has also established the existence of multi-nucleon mechanisms. We must now focus on precision measurements of this type, in specific regions of phase space, in order to determine the exact nature of the reaction and its precise contribution to (e, e') reactions.

- In the experiment described in this proposal, pp and pn events will be detected **simultaneously** using HARP and the Hadron HRS. Consequently, the data for short-range correlations in the pp-channel will be taken at the same time as the measurements of correlations in the pn-channel, thus determining both components of the one- and two-body mechanisms.

- The measurement of both pp- and pn-channels **must** be made with adequate kinematical constraints to separate MEC and IC contributions in the reaction mechanism. This requires an L/T separation, even in the pp-channel which has a small cross section, and as a result the experiment must be able to handle

high luminosities. Discrete detectors (with a good S/N ratio) are ideally suited to such conditions as compared to "phase space" 4π-detectors.

- The pp-channel may provide the cleaner signature of short range correlations, however, the pn contribution **must** be accurately measured, because it dominates the ^{3}He break up reaction and it will interfere with the pp-channel. The latter is approximately 10 % of the pn-channel while the FSI in the pn-channel, mimicking pp emission, is of the same order.

- Since the reaction ^{3}He(e,e'pn)p is kinematically complete, neutron detection, with adequate efficiency and resolution, will determine **both** 2NA and 3NA strengths simultaneously by restricting the data analysis in the phase space regions corresponding to 2NA and 3NA kinematics, respectively. Similar analysis of the same data set can be used to search for and determine 3BF contributions. All these processes of interest in ^{3}He are coplanar by nature, thus negating any advantage 4π solid angle detectors are perceived to enjoy. These detectors are ideally suited to multi-particle detection and out-of-plane effects.

- A final advantage of performing this experiment with HARP in Hall-A arises due to the polarization capability of this device. At no extra cost, the spin of the nucleons is automatically analyzed. Although this is not a principle aim of this proposal, it should be realized that the acquired asymmetry data can be analyzed off-line, and with proper theoretical support, information can be extracted on aspects, such as FSI, which strongly affect specific polarization amplitudes.

2.4.2 Conclusions

The ^{3}He(e,e'pp)n and ^{3}He(e,e'pp)n reactions are valuable tools to investigate two-particle wave functions in nuclei, the two-hole spectral density function and the two-body density matrix. The question of short-range correlations is a central issue in nuclear physics, as is the question of the reaction mechanism in (e,e') reactions beyond the elementary e$-$N interaction. The choice of ^{3}He allows the determination of three-body absorption strength and will provide data to test the 3BF question. The configurations chosen and the statistics aimed for, will address such questions related to the reaction mechanism and the nucleon correlations. The detectors available in Hall A, the luminosities expected and the choice of ^{3}He as a nucleus, allow the achievement of the above mentioned goals.

3 Experiment

3.1 The ^{3}He(e, e'pp) Reaction

We have chosen kinematic geometries in regions of phase space where the cross sections are expected to be large, and the description of the knock-out process is simplified. It is important to measure both the epp and enp reactions because each selectively emphasizes different contributions to the cross section and both these measurements can be performed simultaneously with HARP. Restrictions on the kinematics arise from the detector thresholds and the fact that they must not physically overlap.

The count rates have been estimated for ^{3}He(e, e'pp) assuming that the virtual photon couples to a single proton of the correlated pair as shown in Figure 1b. Pion and real photon absorption in the Δ region, show that the np-channel is about 20 times stronger than for pp. Hence, as far as statistics are concerned the pp-channel is normally the limiting one, and we therefore concentrate on it. Only the plane wave (PW) longitudinal cross section for this process has been calculated, under the rationale that the transverse component does not contribute to first order. The code of Laget [39] has been used for this purpose, and to evaluate the accuracy of the resulting cross sections, selected kinematics were also run using the code of Tjon [37]. The two codes are in reasonable agreement: as an example, for E_o = 570 MeV, ω = 200 MeV, q = 282 MeV/c and in parallel kinematics, Tjon produced a PW-longitudinal cross section for the pp-channel twice as large as Laget's, while the transverse cross sections agreed within 50%.

In the estimate of the counting rates the rescattering of the nucleons or final state interactions are not included, and the residual nucleon is treated as a spectator with zero momentum. Two different configurations are considered, with the two protons being emitted:

- back to back in the laboratory (anti-parallel), and
- symmetrically, with the absorbed virtual photon bisecting the angle between the two ejected protons.

To summarize, the initial momentum of the pair is zero in the laboratory, the neutron behaves as a spectator, the virtual photon is absorbed only on one proton, and the center of mass of the pair lies along the direction of the momentum transfer.

3.1.1 Symmetric Kinematics

This configuration has the advantage that both protons have equal momenta before and after the collision. In other words, there is no ambiguity in the sampling of momenta in the correlation function, which is directly proportional to the cross section in PWIA. In the other configuration, two protons of different initial momenta are being sampled, which however correspond to two indistinguishable protons of the

same momentum being detected. The lower initial momenta are more sensitive to MEC and FSI, while the higher are sensitive to correlations. Combined measurements in anti-parallel and symmetric configurations and theoretical input are thus needed to unfold the various mechanisms.

Using Laget's code [39], cross sections were calculated for various electron beam energies and electron scattering angles, resulting in a range of energy and momentum transfer, and initial proton momenta in the cm-system.

The high energy nucleons will be detected in HARP, which will be placed at forward angles. This is done in order that the somewhat higher threshold of HARP (60 MeV for neutrons and 100 MeV for protons) does not hamper the choice of kinematics. For those kinematics in which the nucleons have kinetic energies exceeding 800 MeV, we have the option to use the hadron (HRSH) spetrometer, if the efficiency of HARP decreases too much. For all other cases, the HRSH will be placed at backward angles and will detect low energy protons.

HARP has an efficiency of 3 %. This is not a hindrance for neutron detection, since the np-channel has large cross sections. This efficiency applies as well to protons, and its adverse effect is mostly negated by operating at a high luminosity. The use of a dedicated proton detector such as the Hadron-IV device (developed and built by the Vrij Universiteit and NIKHEF-K in the Netherlands), is being evaluated as a possible substitute for HARP, in connection to some pp-measurements. Hadron-IV has a nominal solid angle of 500 msr, but it would be employed at a large distance from the target, in order to cope with the high luminosity, thus reducing the effective solid angle to the order of 5 msr. The use of Hadron-IV depends on its performance in a high luminosity environment, which will be established in the coming two years at AmPS.

The chosen kinematics, cross sections and count rates are shown in table 1 below, where the five-fold differential cross section is expressed in $\mathrm{pb/(MeV/c)^2/sr^3}$. The momentum acceptance of the electron and proton spectrometers was taken to be $\Delta p/p = 10$ %, the luminosity was $2.25 \times 10^{38}\ \mathrm{cm^{-2}s^{-1}}$, and the detector solid angles were [42]: $\Delta\Omega_e(8^\circ) = 4.9$ msr, $\Delta\Omega_e(15^\circ) = 7.9$ msr, $\Delta\Omega_{p_l} = 16.0$ msr and $\Delta\Omega_{\mathrm{HARP}} = 50$ msr. The luminosity of $2.25 \times 10^{38}\ \mathrm{cm^{-2}s^{-1}}$ corresponds to a beam current of 150 μA on a high pressure ^{3}He gas target of density 1.20 $\mathrm{g/cm^2}$.

3.1.2 Anti-parallel Kinematics

Following the absorption of the photon the two protons are ejected back to back (180° apart) in the laboratory. This geometry has the advantage of minimizing final state interactions between the ejected protons, since they leave in opposite directions. This is the geometry in which the L/T separation will be carried out, since only the longitudinal and the transverse response functions contribute to the cross section. The longitudinal component is the most sensitive indicator of correlations. An initial set of these kinematics are shown in table 2, which is being refined with the aid of theoretical calculations, since their requirements are stringent and difficult to

Table 1: Count Rate Estimates for Symmetric Kinematics

E_e GeV	ω MeV	q MeV/c	θ_e	p_i MeV/c	T_i MeV	θ_1	θ_2	$d^5\sigma$	rate hr^{-1}
2	200	565	16	436	96	-11.9	-111.1	0.0763	3022
2	300	375	7	544	146	36.3	-103.4	4.0953	120195
4	400	1068	15	638	196	-27.6	-93.8	0.0123	1429
4	500	1097	15	723	246	-15.0	-96.3	0.0099	1267
4	600	1189	16	802	296	-9.9	-94.2	0.0080	1100
4	700	829	7	877	346	32.8	-90.8	0.1660	15257
4	800	912	7	949	396	36.0	-86.6	0.0698	6732

Table 2: Anti-Parallel Kinematics

E_e GeV	ω MeV	q MeV/c	θ_e	ϵ	θ_{cm}	p_1 MeV/c	θ_1	p_2 MeV/c
3.0	900	1076	13	0.91	0	1475.97	-27.10	399.80
3.0					180	399.80	152.90	1475.97
1.3			46	0.44	0	1475.80	-16.48	400.18
1.3					180	400.18	163.52	1475.80
3.5	1200	1348	12	0.90	0	1798.16	-21.55	450.05
3.5					180	450.05	159.46	1798.16
1.9			30	0.58	0	1798.18	-15.46	450.01
1.9					180	450.01	164.54	1798.18

accomplish.

The cross sections for these kinematics were obtained in two ways. For the forward angle of each point, where the longitudinal component dominates, Laget's code was used. At the large electron angle, real photon data [9, 40] was suitably manipulated to effectively yield the transverse component of the reaction in question. This involved using the mass dependent empirical formula for estimating the (γ, p) cross sections together with the $^9Be(\gamma, pn)$ and $^9Be(\gamma, pp)$ angular correlation data [40]. The resulting figures were checked against the $^3He(\gamma, p)$ results from reference [9] and were found to be in agreement.

3.2 The ^{3}He(e, e'np) Reaction

It is well known from pion and real photon absorption experiments, that the (e, e'np) cross sections are about 10 to 20 times larger than the corresponding cross sections of the pp-channel. The PW calculations of Laget and Tjon indicate precisely the

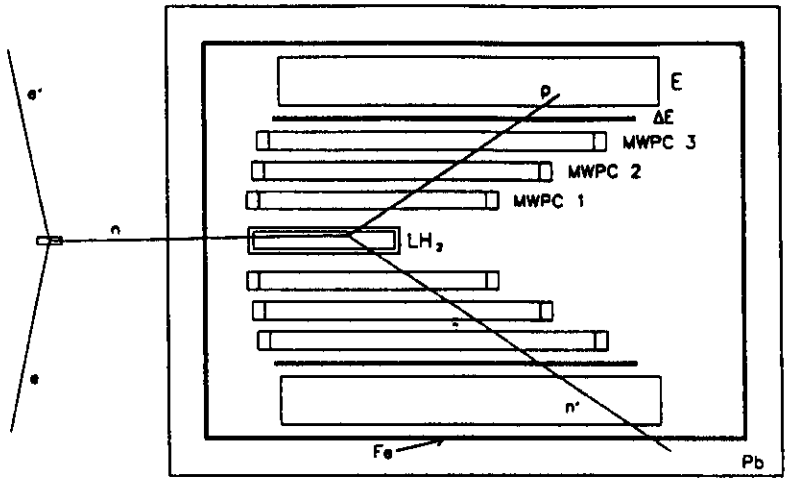

Figure 15: A schematic representation of the geometry for HARP.

same fact, and the two codes agree to a level of 10 % on the np/pp ratio. Hence, since protons and neutrons will be detected simultaneously, the desired statistical precision is defined by the pp-channel.

3.3 Singles and Accidental Coincidence Rates

Detailed calculations of the singles and accidental counting rates involving HARP and the HRS[2] spectrometers are in progress. A Monte Carlo physics event generator (ENIGMA [41]) feeds the GEANT detector simulation package. No background problems are anticipated due to the triple-coincidence between these three devices and the inherent low-noise of HARP (which employs at least a four-fold internal coincidence).

3.4 The HARP Neutron Polarimeter

3.4.1 Principle of Operation

HARP operates on the recoil principle. Its design is based on $\Delta E - \Delta E - E$ scintillator detector telescopes and tracking devices (Multi Wire Proportional Chambers, MWPC) placed around the converter, which contains liquid hydrogen (LH_2). Eight such telescopes and three MWPCs will be positioned at either side of the converter (see Figures 15 and 16).

HARP can be used for protons as well, since they also scatter in the converter, and both scattered and recoil protons can be subsequently detected. HARP can detect both incoming protons and neutrons simultaneously by employing an "intelligent" trigger, and a charged particle tagger between the target and the converter.

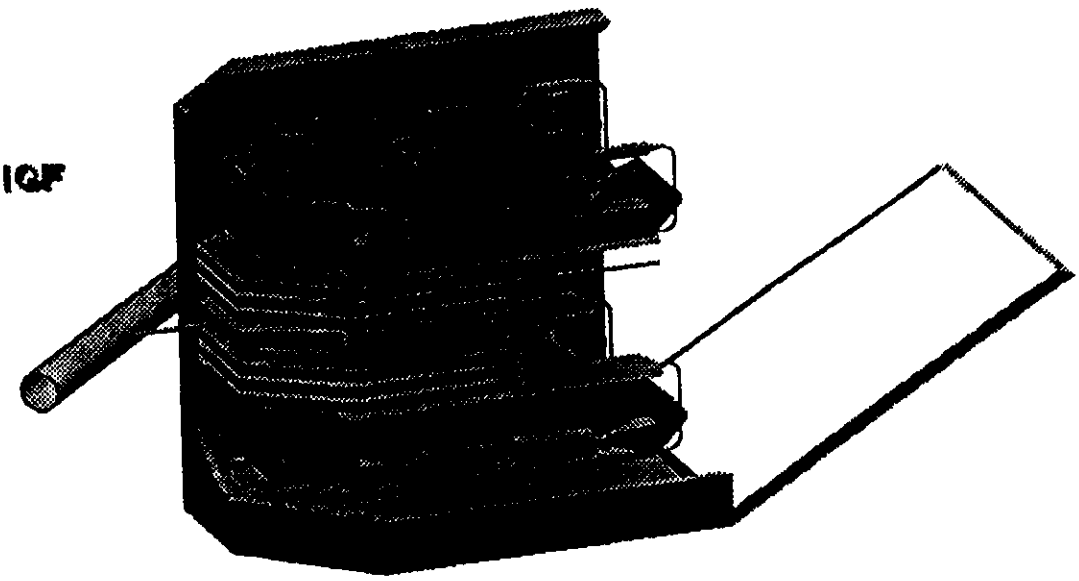

Figure 16: A three-dimensional representation of HARP. Also visible is the beam pipe (slanted cylinder) and the drop-down rear wall of surrounding shielding house).

Selected results of the simulations serve to illustrate the expected performance of HARP [43]. The efficiency is approximately 3 %, and remains roughly constant as a function of the nucleon kinetic energy. The energy resolution ($\Delta T_n/T_n$) is modest (8 %), but it also remains relatively constant up to 800 MeV nucleon energy. Simulations are underway to determine whether these properties change significantly in the range from 800 to 1200 MeV. These characteristics are coupled to a very high insensitivity to background, and hence the tolerance of a very high luminosity.

3.4.2 The Design of HARP

The design of HARP is described in detail elsewhere [44]. A trapezoidal shape has been chosen for the LH_2 converter, of 3 cm height and 60 cm depth (along the path of the neutron). The front and rear sides are 80 cm wide and 150 cm wide, respectively, yielding a large surface area. This sheet will contain about 25 liters of LH_2. A prototype vessel is under construction at NIKHEF-K and will be soon tested together with the cryo-system.

The HARP detectors can be setup in two orientations: the scintillator walls being horizontal (U-D configuration), or vertical (L-R). The former will be employed in this experiment since it offers the maximum solid angle of HARP, 50 msr. In this configuration the minimum angle with respect to the beamline which can be reached is 45°. For this angle, HARP can simultaneously measure particles from 15° to 75°.

The E-counters will have a thickness of 20 cm, and can thus stop up to 175 MeV perpendicularly impinging protons. The two ΔE detectors are 3 mm and 10 mm thick, respectively. The ΔE layers allow for a secure proton identification down to 18 MeV, and "tighten" the trigger level for proton energies beyond 40 MeV. A

charged particle tagger will be positioned in front of the converter, to discriminate between incoming protons and neutrons, and will consist of two overlapping planes of narrow plastic scintillator strips equipped with small photomultiplier tubes.

The detectors will be enclosed in a 6 cm thick lead-steel house to be shielded from background. The total weight for HARP is estimated at 25 tons which includes a platform to allow for rotation around the target center-post.

3.4.3 The Merits of HARP

The recoil principle leads to a large background suppression by eliminating photons and low energy neutrons, and it permits recoil detectors to operate at much higher luminosities than TOF detectors. This is partly a result of shielding the sensitive detectors: they do not "look" directly at the target (which is also a source of unwanted background events) but are placed behind walls. In addition, the high-fold coincidence required to detect the proton (four wire chamber planes and two scintillators) further reduces the neutral background. Finally, measurements of the energy and time variables of the detected particles are carried out independently. In this manner, the two variables may be used to cross check each other, effectively compressing the neutron TOF spectrum into a narrow peak, hence improving the S/N ratio. HARP will thus operate at a much higher luminosity than other n-detector system. This reduces the experimental beam time needed in order to obtain the required statistical precision, or conversely allows the measurement of processes with much lower cross sections.

A final advantage of HARP is that it is relatively easy to calibrate with respect to the efficiency of detection and of n-p conversion. This procedure involves the determination of the wire chamber efficiency in a pairwise cyclic manner, while the scintillators may be calibrated in situ with a reaction of known kinematics and cross section (e.g. via ^{1}H(e, e'p) with the protons detected in HARP). The PMT gain will be continuously monitored with a flasher ADC/fiber optic system, coupled to a counter which is continuously referenced to an ^{241}Am source.

HARP will be commissioned at AmPS using an unpolarized electron beam in mid-1994. Measurements on ^{1,2}H targets will be performed, in which the electron elastically scatters from the proton and respectively the neutron, and both the scattered electron and the nucleon are detected. These measurements will serve to get the instrument fully operational and will provide a check of the calibration procedure. The device will be shipped to Hall-A as dictated by the physics interest of the HARP and Hall-A collaborations and depending on the experimental scheduling.

3.5 The Primary Target

Targets for this experiment and related experiments are being currently designed and constructed. These designs call for cryogenic gas targets to be operated at a high pressure. The design addresses the issues of the required high density to achieve

Table 3: Beam Time Estimate for Symmetric Kinematics

E_e GeV	ω MeV	q MeV/c	rate hr^{-1}	HRSH bins	HARP bins	Time hours
2	200	565	3022	2	5	110
2	300	375	120195	2	5	3
4	400	1068	1429	2	5	230
4	500	1097	1267	2	5	260
4	600	1189	1100	2	5	300
4	700	829	15257	2	5	20
4	800	912	6732	2	5	50
					Counting time	973

luminosities of 10^{38} $cm^{-2}s^{-1}$, the large amounts of heat deposited by the beam in the target, the high energy densities at the interaction region due to the small size of the beam spot, the containment of density flucutations due to beam heating and minimizing the thickness of the target cell windows.

A preliminary design for a ^{3}He cell specifies a minimum operating temperature of 20 K and pressure of 70 atm. The corresponding target gas density is 80 mg/cm^3. For an effective cell length of 15 cm (perpendicular), luminosities of 10^{38} can be achieved for beam currents of 50-150 μA. For a cylindrical cell of 15 cm (physical) length with spherical end caps, a wall thickness of 0.03 cm of aluminum 7075-T6 is being incorporated in the current design. This design specifies that the target cell be viewable by two spectrometers simultaneously (one on each side of the beam pipe), over an angular range of $10° - 130°$ in the scattering plane and $\pm 10°$ out of plane. The latter figure is more than sufficient as far as HARP is concerned, since this device will have a $\pm 3°$ out of plane acceptance in its U-D configuration.

The bulk power dissipation in the target will be dealt with a L^{4}He refrigerator and a suitable heat exchanger. For the ^{3}He target cell, a maximum power dissipation of 1.0 kW (for a 200 μA beam) is anticipated. To minimize density variations due to local beam heating, the target material will flow transversely past the beam with velocities up to 10 m/s.

The group from California State University is involved in the design of these targets, in consultation with John Mark, a target specialist at SLAC.

3.6 Beam Time Estimate

The count rates were based on PW cross sections, since as was mentioned above, the FSI contribution appears to be small. We wish to observe the complete proton spectrum for each 10 % byte in the electron momentum of the HRSE spectrometer. Assuming 100 MeV/c bytes, the momentum range in the proton spectrometer can

Table 4: Beam Time Estimate for Anti-Parallel Kinematics

E_e GeV	ω MeV	q MeV/c	ϵ	rate hr^{-1}	HRSH bins	HARP bins	Time hours
3.0	900	1076	0.91	198	2	10	101
1.3			0.44	81	2	10	248
3.5	1200	1348	0.90	225	2	10	89
1.9			0.58	96	2	10	209
						Counting time	647

Table 5: Total Beam Time Estimate

	hours
Symmetric kinematics	973
Anti-Parallel kinematics (L/T)	647
Setup, calibration, angle changes	300
Total time	1920

be covered in 2 bins. In the L/T case (anti-parallel) a finer binning was taken for HARP to reflect the higher accuracy desired in these measurements. Assuming a desired 1000 counts/bin, we arrive at the counting times shown in tables 3 and 4. According to these calculations, the amount of running time is 1620 hours. Adding 300 hours for setup time, testing, angle and energy changes, and contingency brings the total beam time request to 1920 hours (table 5). These numbers have been calculated assuming operation at a luminosity of 2.25×10^{38} $cm^{-2}s^{-1}$ and a 3 % efficiency for HARP.

4 Acknowledgements

We wish to thank M.J. Dekker for his comments on the proposal and useful discussions on theoretical aspects of the proposal.

References

[1] S. Auffret et al., Phys. Rev. Lett. **55** (1985) 1362.

[2] G. van der Steenhoven et al., Nucl. Phys. **A480** (1988) 547.
J.B.J.M. Lanen et al., Phys. Rev. Lett. **64** (1990) 2250.

[3] P.E. Ulmer et al., Phys. Rev. Lett. **61** (1988) 2001.
P.E. Ulmer et al., Phys. Rev. Lett. **59** (1987) 2259.

[4] Z-E. Meziani et al., Phys. Rev. Lett. **54** (1985) 1233;
Z-E. Meziani et al., Phys. Rev. Lett. **52** (1984) 2130.

[5] C. Marchand et al., Phys. Rev. Lett. **60** (1988) 1703.

[6] J. Ahrens et al., Phys. Lett. **146B** (1984) 303.

[7] P. Carlos et al., Nucl. Phys. **A431** (1984) 573.

[8] T. Emura et al., The TAGX collaboration, Phys. Rev. Lett. (submitted).

[9] G. Adams et al., The LEGS collaboration, private communication (1993).

[10] P. Weber et al., Phys. Rev. **C43** (1991) 1553.

[11] P. Weber et al., Nucl. Phys. **A534** (1991) 541.

[12] J.D. Silk, Phys. Rev. **C37** (1988) 891.

[13] H. Baghaei et al., Phys. Rev. **C39** (1989) 177.

[14] R.D. McKeown et al., Phys. Rev. Lett. **44** (1980) 1033.

[15] Th.S. Bauer, Invited talk at the International Workshop with BLAST, Tempe, Arizona, March 1992 to be published.
A. Zondervan, Ph.D. Thesis, University of Amsterdam, unpublished (1992).

[16] M.J. Dekker et al., Phys. Lett. **289B** (1992) 255.

[17] R.W. Lourie et al., Phys. Rev. Lett. **56** (1986) 2364.

[18] T. Takaki, Phys. Rev. Lett. **62** (1989) 395.

[19] H. Primakoff and T. Holstein, Phys. Rev. **55** (1939) 1218.

[20] J.M. Laget, Phys. Rev. **C38** (1988) 2993;
J.M. Laget , J.Phys. G: Nucl. Phys. **14** (1988) 1445 .

[21] S. Coon and B. Friar, Phys. Rev. **C34** (1986) 1061.

[22] A.J. Sarty, Nucl. Phys. **A543** (1992) 49;
N.R. Kolb et al., Western Regional Nuclear Conference, Lake Louise, February 1993 (unpublished).

[23] G. Audit et al., Phys. Rev. **C44** (1991) R575.

[24] H. Arenhovel and M. Sanzone, Few Body Systems Suppl. 3, Springer Verlag, Wien, N.Y.

[25] G.E. Brown et al., Phys. Lett. **118B** (1982) 39;
B. Schwesinger et al., Phys. Lett. **132B** (1983) 269.

[26] E. Oset et al., Nucl. Phys. **A448** (1986) 597;
M.J.V. Vacas and E. Oset, private communication (1993);
L.L. Salcedo et al., Nucl. Phys. **A448** (1988) 557.

[27] S. Barshay and D. Rein, Zeit. fur Phys. **C46** (1990) 215; S. Barshay, Mod. Phys. Lett. **A5** (1990) 107.

[28] W. Kratschmer, Nucl. Phys. **A298** (1978) 477.

[29] S. Boffi, Proceedings of the Topical Workshop on Two-nucleon Emission, ed. O. Benhar and A. Fabrocini (ETS editrice, Pisa, 1991) 87.

[30] G. Orlandini and W. Leidermann, private communication.

[31] C. Giusti et al., Nucl. Phys. **A546** (1992) 607.

[32] C. Giusti and F.D. Pacati, Nucl. Phys. **A535** (1991) 573.

[33] H. Yokota et al., Phys. Rev. Lett. **58** (1987) 191.

[34] Z. Papandreou et al., Phys. Lett. **227B** (1989) 25.

[35] G.J. Lolos, TRIUMF experiment E555 (1989).

[36] C.L. Morris and R.D. Ransome, "Pion Absorption on Light Nuclei", LAMPF Progress Report LA-12256-PR (1990) 17.

[37] E. van Meijgaard and J.A. Tjon, Phys. Rev. **45** (1992) 1463.

[38] S. Boffi and M.M. Giannini, Nucl. Phys. **A533** (1991) 441.

[39] J.M. Laget, Phys. Rev. **C35** (1987) 832.

[40] M. Kanazawa et al., Phys. Rev. **C35** (1987) 1828.

[41] J.L. Visschers, ENIGMA Monte Carlo, version 2.4, unpublished (1993).

[42] J. Le Rose, CEBAF, private communication (1989).

[43] H.W. Willering, "Optimization of the HARP Detector", Utrecht Internal Report V(SAP) 92-14, October 1992.

[44] Z. Papandreou et al., "High Acceptance Recoil Polarimeter", CDR v2.0, Utrecht University Internal Report, August 1992.